Low Temperature Physics/Fizika Nizkikh Temperatur, 2016, v. 42, No. 10, pp. 1129–1136

Magnon–phonon coupling and implications for charge-density wave states and superconductivity in cuprates

Viktor V. Struzhkin

Geophysical Laboratory, Carnegie Institution for Science, 5251 Broad Branch Road NW, Washington DC 20015, USA
E-mail: vstruzhkin@carnegiescience.edu

Xiao-Jia Chen

Center for High Pressure Science and Technology Advanced Research, Shanghai 201203, China

Received May 20, 2016, published online August 29, 2016

The mechanism of high-temperature superconductivity of copper oxides (cuprates) remains unsolved puzzle in condensed matter physics. The cuprates represent extremely complicated system, showing fascinating variety of quantum phenomena and rich phase diagram as a function of doping. In the suggested "superconducting glue" mechanisms, phonon and spin excitations are invoked most frequently, and it appears that only spin excitations cover the energy scale required to justify very high transition temperature $T_c \sim 165$ K (as in mercury-based triple layer cuprates compressed to 30 GPa). It appears that pressure is quite important variable helping to boost the T_c record by almost 30 degrees. Pressure may be also considered as a clean tuning parameter, helping to understand the underlying balance of various energy scales and ordered states in cuprates. In this paper, a review of mostly our work on cuprates under pressure will be given, with the emphasis on the interactions between phonon and spin excitations. It appears that there is a strong coupling between superexchange interaction and stretching in-plane oxygen vibrations, which may give rise to a variety of complex phenomena, including the charge-density wave state intertwined with superconductivity and attracting a lot of interest recently.

PACS: **74.72.–h** Cuprate superconductors;
74.25.nd Raman and optical spectroscopy;
74.62.Fj Effects of pressure.

Keywords: high-T_c superconductivity, charge-density wave, pressure effect.

1. Introduction

Recent experiments have discovered a charge-density wave (CDW) state in several families of high-T_c cuprates, predominantly in underdoped materials [1–11]. The mechanism behind the CDW state formation is not clear, but the importance of the CDW state for the understanding of high-T_c superconductivity is widely acknowledged, with opinions ranging from the competition scenario [2] to the symbiotic views of intertwined CDW state and superconductivity [10].

The CDW state, predicted by Peierls in 1930, has been discovered experimentally, and presents another fascinating example of macroscopic quantum state (see review papers for details [12,13]), similar in that respect to a superconducting state, albeit with different properties. The CDW state is gapless and is usually pinned to the lattice imperfections. It has fascinating transport properties: if applied voltage is above the pinning threshold, non-ohmic conductivity and generation of oscillating currents are observed, similar to Josephson effect in superconductors [13].

In this paper, we will review experimental evidence from high-pressure experiments that supports strong coupling between lattice and spin excitations in cuprates, and we will also discuss pressure effects on superexchange interactions in cuprates and the relevance of the superexchange interactions as proper "superconducting glue" in the cuprates.

2. Pressure effect on phonon and magnon excitations and pressure-induced insulator–metal transition in cuprates

It is not an easy task to measure experimentally spin excitations in a material under conditions of high pressure. However, it has been discovered a while ago, that two-magnon excitations (a simultaneous flip of two neighboring spins) can be measured in various materials by Raman scattering [14,15], cuprates being no exception [16,17].

Raman scattering is a very convenient technique for application with diamond anvil cell (DAC) pressure devices [18]. Indeed, few experiments have been reported at high pressure, probing antiferromagnetic interaction in NiO [19], K_2NiF_4 [20], and also in parent high-T_c compounds by measuring two-magnon Raman scattering. In one of our papers, we have measured two-magnon Raman scattering [21] in a single layer parent antiferromagnetic cuprate Eu_2CuO_4. In another experiment, we utilized another powerful tool for probing magnetic interactions — infrared absorption — to measure coupled phonon-multimagnon excitations in $Sr_2CuCl_2O_2$ material [22] (two-magnon and four-magnon excitations coupled to phonons were measured). To understand underlying physics, a brief summary of two-magnon Raman experiments and theoretical treatments is given below.

2.1. Two-magnon Raman scattering

The search for the mechanism of high-temperature superconductivity related to magnetic excitations and/or superexchange interaction J justifies interest to 2-magnon Raman scattering, which directly probes J. It was found [17] that the linewidth of 2-magnon Raman line is not described by the spin wave theory [15]. Further theoretical considerations [23] revealed that for $S = 1/2$ antiferromagnet quantum spin fluctuations are responsible for the anomalously broad two-magnon Raman line. Our work [21] on Eu_2CuO_4 and experiments [24] on two-magnon Raman scattering in La_2CuO_4 provided estimates of pressure dependence of superexchange integral $J \sim \omega(2M)/2.7$ [here $\omega(2M)$ is the frequency of 2-magnon Raman excitation — see Ref. 23. It was found that scaling of the exchange integral J with the Cu–O distance d is given by

$$J \sim d^{-n} \tag{1}$$

with n ranging from 3 to 5, which deviated significantly from the empirical $n \sim 10$–12 relation [25] for many antiferromagnetic compounds.

Cooper and coworkers [26] proposed the explanation of the anomalous bond length dependence which followed from their experimental findings on M_2CuO_4 where M = Pr, Nd, Sm, Eu, Gd. They used well known [27] expression for superexchange

$$J = \frac{4t^4}{\Delta^2}\left(\frac{1}{U} + \frac{1}{\Delta}\right) \tag{2}$$

(Δ — charge transfer gap, U — Mott–Hubbard gap), and it was found that $J \sim d^{-(4\pm2)}$.

2.2. Infrared absorption

Similar scaling $J \sim d^{-4}$ was found for $Sr_2CuCl_2O_2$ in our infrared absorption experiments [22]. These measurements confirmed previous assignment of higher-energy bands (at ~4000 cm^{-1}) to four-magnon excitations (see Fig. 1). Three different mid-infrared (MIR) optical absorption bands were discovered in the insulating single-layer spin-1/2 cuprates (R_2CuO_4 and $Sr_2CuO_2Cl_2$) by Perkins *et al*. [28]. These MIR bands consist of one sharp peak near 2800 cm^{-1} (~0.35 eV) with two broad higher-energy sidebands. The first sideband, centered near 4000 cm^{-1} (~0.5 eV), dominates their spectral weight. These bands were shown to be intrinsic excitations of the CuO_2 layers, and have since been observed in bilayer cuprates [29]. To our knowledge, only cuprates are known to display this full set of excitations. The MIR excitations were originally attributed to a crystal field exciton with one- and two-magnon sidebands [28]. However, cluster calculations do not predict an exciton in this energy range. An alternate explanation for their origin was provided by Lorenzana and Sawatzky (LS) [30,31]. They proposed that the sharp ~0.4 eV peak corresponds to the absorption of one optic phonon plus a different quasiparticle excitation of the Heisenberg Hamiltonian consisting of a long-lived quasibound state of two magnons — "bimagnon". Their calculated line shape closely fits the measured peak. While composite two-magnon phonon excitation has previously been observed in NiO, it is not a virtual bound state and hence is much broader in energy [32]. Apparently, an analogous two-spinon one-phonon excitation was observed in one-dimensional (1D) Sr_2CuO_3 [33]. However, the sidebands are absent in both NiO and Sr_2CuO_3. LS further speculated that the two higher-energy sidebands were four-magnon one-phonon (4Mph) excitations (with magnons arranged either in a plaquette or a row), an excitation which appears to have not been observed in any non-cuprate material. LS note that these sidebands are a consequence of quan-

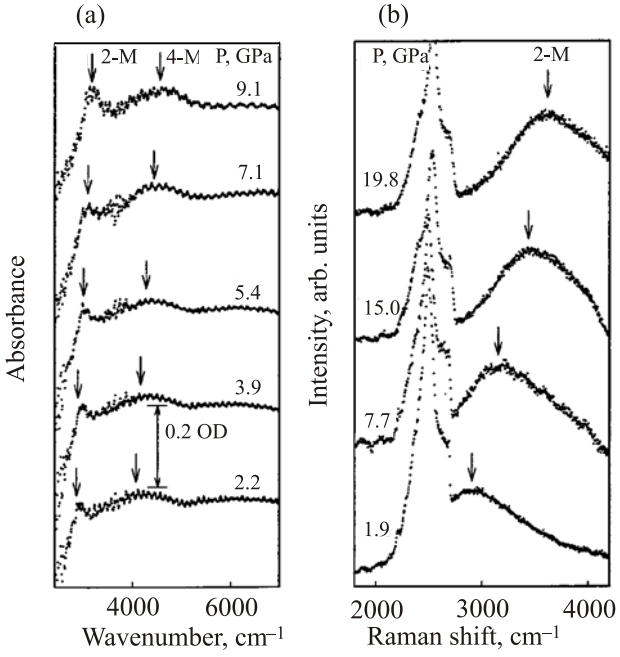

Fig. 1. Room-temperature MIR absorption and two-magnon Raman scattering spectra in SCOC at several pressures. The spectra are vertically offset for clarity [22].

tum fluctuations in the spin-1/2 cuprates, although ordinarily their optical absorption strength would be so weak as to be barely observable. Indeed, numerical calculations predict 4MP sidebands to be very weak for the cuprates, with spectral weight just ~3% of the bimagnon. However, the experimental data are in stark contrast with this expectation, with the sidebands being ~10^2 times larger than calculated. The first sideband has nearly three times the spectral weight of the putative bimagnon. In the LS model, the symmetry-breaking phonon is crucial to the appearance of multimagnon excitations, as the crystal structure has inversion symmetry. Without the phonon, magnon pairs are electric dipole forbidden. The specific phonon involved is the Cu–O stretch (breathing mode), which modulates the Cu–O bond length and hence the superexchange coupling J. Consequently, this phonon strongly interacts with magnons. We also argued that there are reasons to believe that the coupling of he Cu–O stretch phonon (ph) to the four-magnon (4M) may be anomalous in the cuprates. In this regard the spin-1/2 cuprates are special, as quantum fluctuations are maximal and the exchange coupling is unusually strong. Hence four-magnon creation is quantum enhanced and the magnon–phonon coupling energy is unusually large. For these reasons, composite 4Mph excitation may have an effective charge much larger than perturbation theory would predict. It is insightful to examine the 4Mph bond textures (in real space) that result from different 4M and ph wave vectors.

From this simple approach, it is clear (via examination of the affected bonds) that the 4Mph interaction is attractive. To couple to a $\mathbf{q} = 0$ photon the 4M (ph) must have wave vector $+\mathbf{Q}$ ($-\mathbf{Q}$), with maximal density of states when $\mathbf{Q}$ is on the zone boundary. For $\mathbf{Q} = (\pi/a,\pi/a)$, the plaquette of 4 flipped spins favors the same bond variations as the "breathing mode" phonon with $-\mathbf{Q}$. Similar attraction occurs at $\mathbf{Q} = (0,\pm\pi/a)$ or $(\pm\pi/a,0)$ (antinodal points), where the 4Mph resembles dimerized rows, possibly signaling latent tendencies within the undoped insulator that contribute to stripe/CDW formation once doped holes are introduced.

2.3. Insulator–metal transition Bi2212: coupling, anomalies, critical points, effects of doping

We have reviewed above the evidence for strong coupling between spin excitations and phonons in parent cuprate compounds. However, it is well known that doping strongly modifies spin properties in cuprates, suppressing magnetic order in underdoped regime, and completely de-

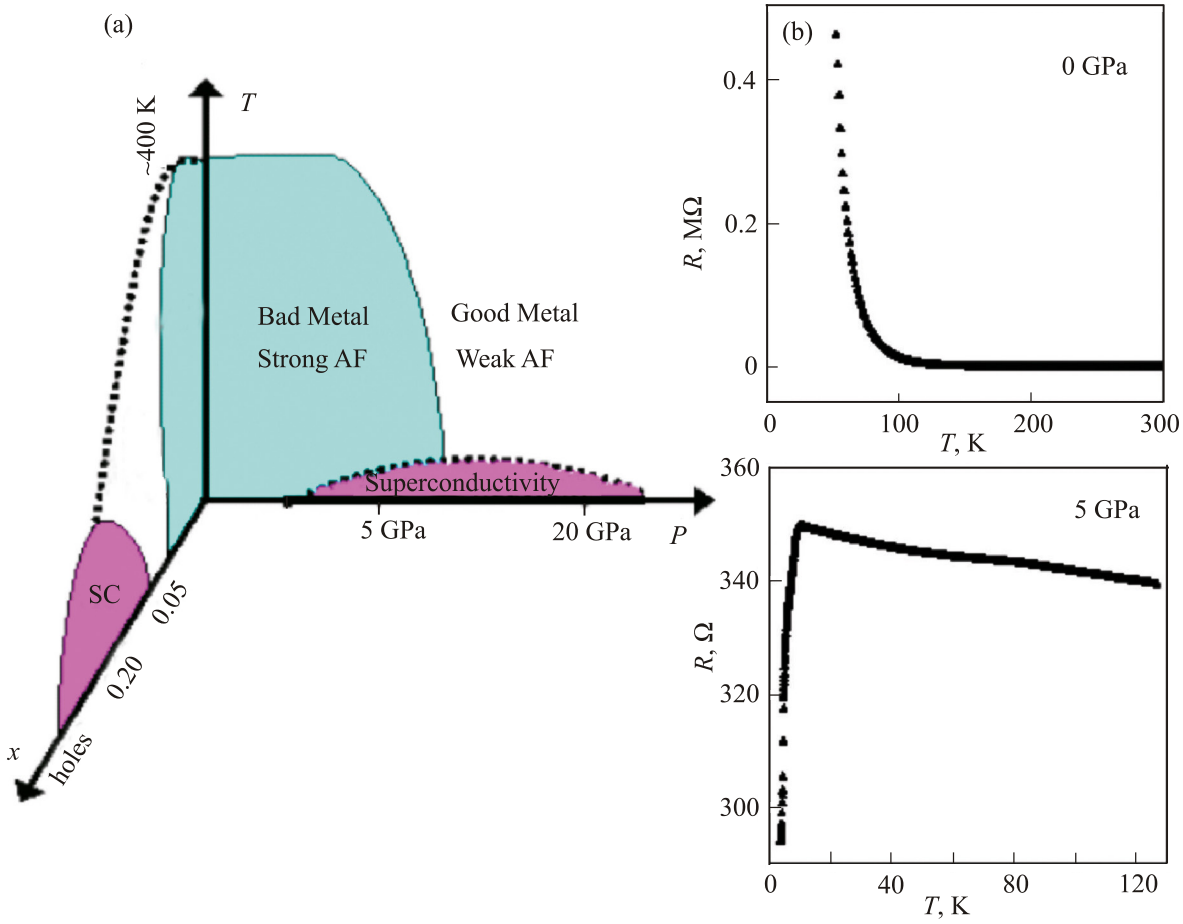

Fig. 2. (Color online) Insulator–metal transition in $Bi_{1.98}Sr_{2.06}Y_{0.68}Cu_2O_{8+\delta}$ under pressure. (a) Tentative phase diagram, comparing doping to pressure variable. It is assumed that effect of pressure could be modeled by continuous injection of holes into CuO_2 planes. (b) Superconducting transition in the sample compressed to 5 GPa, compared to insulating behavior at ambient pressure.

stroying antiferromagnetic fluctuations in the overdoped cuprate materials. To clarify the effect of doping, we have measured a $Bi_{1.98}Sr_{2.06}Y_{0.68}Cu_2O_{8+\delta}$ samples, which are doped to be close to the metallic state, but on the insulating side of the phase diagram [34]. The samples have been compressed through the insulator–metal transition, which was observed below 20 GPa, and significant anomalies have been detected in phonon and magnon excitations.

We show the tentative phase diagram and pressure-induced superconductivity in Fig. 2. The sample became superconducting at 5 GPa, however, both resistance and Raman response did not show metallic behavior until about 20 GPa. Around 20 GPa, both phonon and magnon excitations have quite significant anomalies which point to the possibility of a critical point in the phase diagram at that pressure.

In Fig. 3, the pressure evolution of the two-magnon, and B_{1g} phonon is shown, along with compressibility of the unit cell c and a axes. To plot Raman spectra, we used $1/c$ instead of pressure (Birch-type plot), which usually shows linear mode behavior. Interestingly, both magnon and phonon excitations show deviation from a linear behavior below 10 GPa, possibly close to the transition to superconducting phase. The slope has a tendency to change back to original values when 20 GPa transition is passed.

The transition at 20 GPa is clearly observed in Raman spectra in Fig. 4.

We establish a pressure driven electronic transition through the onset of a linear electronic background and an abrupt increase of electron–phonon coupling at ~20 GPa in the low-T Raman spectra of Fig. 4. The change in conductivity contributes a change of low frequency, linear background

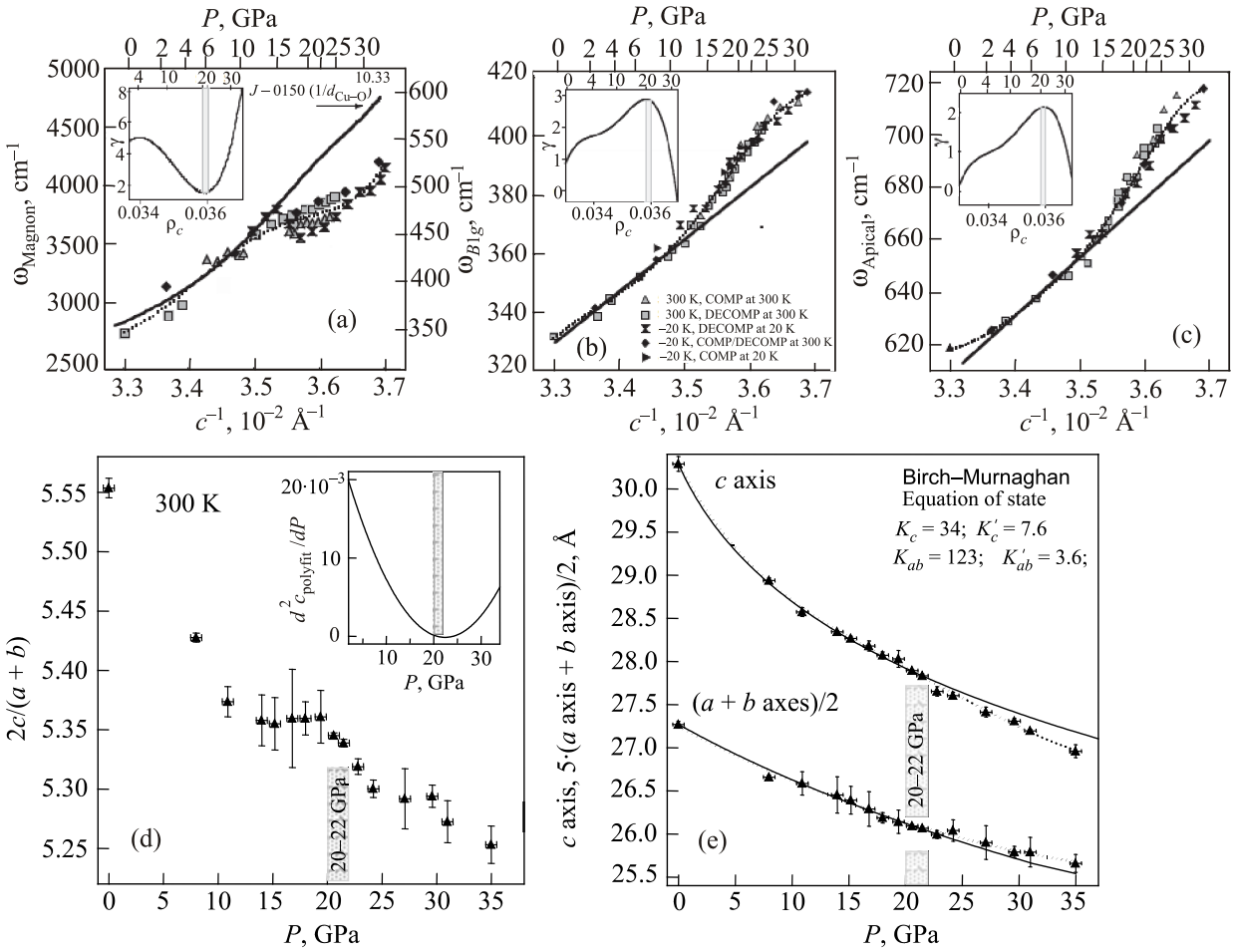

Fig. 3. Peak positions of the two-magnon peak (a), B_{1g} phonon (b), and apical phonon (c), at low (20 K) and high (300 K) temperatures plotted against the c-axis lattice density and pressure. The data was taken with different pressure, temperature pathways indicated by the marker styles. Inset of (a) shows the derivative of a fit to all the data points (dotted curve). Insets of (b) and (c) show the same derivative for the phonons. Solid lines in (b) and (c) are guides to the eye, following the low-pressure dependence. Panels (d) and (e) show c/a ratio and c, a axis, measured by powder x-ray diffraction in Ne pressure medium. (d) Plot of $2c/(a + b)$. (e) The c axis and $5(a + b)/2$ axis lattice constants plotted versus pressure. Solid lines are fits to the Birch–Murnaghan equation of state between 0–20 GPa. Dotted curves are polynomial fits to the entire data range between 0–35 GPa. A second derivative of this polynomial fit for the c axis is plotted in the inset. For more details see [34].

to the Raman cross-section [35,36]. Figure 1(b) shows the results of a linear fit of the electronic background between 200 and 300–350 cm^{-1} — a spectral range below the oxygen B_{1g} phonon — with a sharp onset at ~20 GPa.

Concomitant to this change in the electronic background, the intensity of the B_{1g} phonon decreases significantly and its line shape becomes asymmetric. The full Fano line shape of the B_{1g} phonon was fit using the theory of Ref. 37, giving a sharp increase of $\lambda \sim 0.1$ at ~20 GPa [37]. The sharp change of λ is consistent with an increase of mobile charge carriers in the presence of an unscreened electron–phonon interaction [38]. Upon further increase of metallicity, the electron–phonon interaction becomes screened as in conventional metals, consistent with the downward trend of λ beyond 25 GPa shown in Fig. 4(c). Thus both the electronic background and Fano line shape indicate an abrupt change in conduction at ~20 GPa.

Dramatic softening of two-magnon excitations (Fig. 2) is compatible with increased doping of CuO_2 layers under pressure, if compared to doping dependence invoked from Ref. 39. However, above 25 GPa the magnon and phonon slopes are approaching values below typical 10 GPa. For the magnon slope, we get $n \sim 10$ for a lattice constant, which is a measure d(Cu–O) interatomic distance below 10 GPa (see Eq. (1)) (please note that $n \sim 4.4$, if calculated against compressibility of the c axis), and much lower slope n is found in the pressure region between 10 and 25 GPa, where holes are injected into CuO_2 planes. It also appears from the increased slope in magnon dependence versus reciprocal lattice constant, that hole injection slows down significantly above 25 GPa. Comparing to previous data on Eu_2CuO_4, La_2CuO_4, and $Sr_2CuCl_2O_2$, the reported reduced pressure dependence of superexchange interaction of these single-layer materials may be explained by the lack of reliable x-ray data for calculation of compressibility of the lattice constant a (compressibility within CuO_2 planes).

The kink in phonon dependencies in Fig. 2 is less clear, we assumed that it is due to increased screening within CuO_2 planes. Further complications arise when we study triple-layer materials [40], but we will restrict ourselves to the simple case of homogeneously doped CuO_2 planes in single- or double-layered materials.

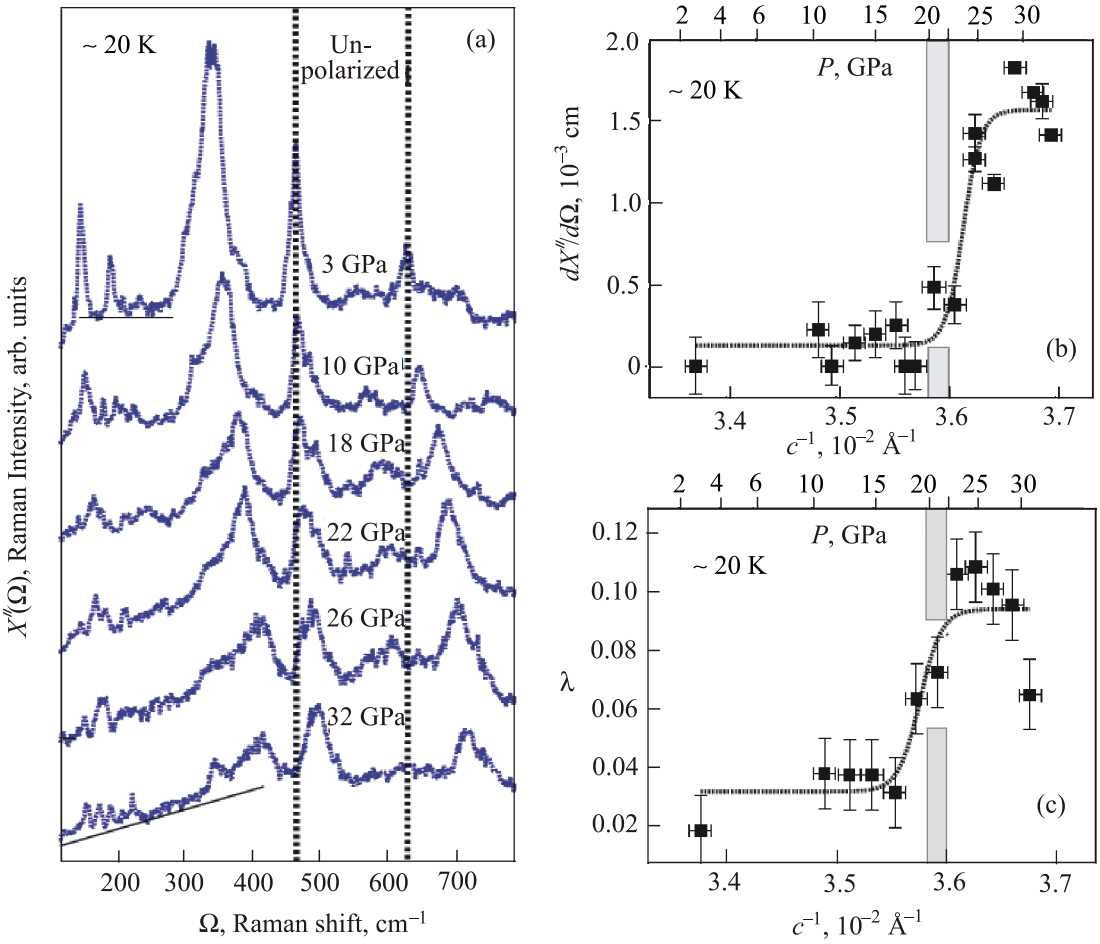

Fig. 4. (a) Raman spectra of the B_{1g} phonon, O_{Bi} phonon in the Bi–O block layer, and the apical oxygen phonon at ~20 K with pressure. Vertical dashed lines are guides to the eye. (b) Slope of the linear electronic background from 200–300 cm^{-1} at ~20 K. Spectra at each pressure were normalized to the intensity at 850 cm^{-1}. (c) The full Raman vertex, using a normal state electronic background, was fit to 20 K data to derive the electron–phonon coupling parameter λ. Procedure in Ref. 25. Vertical grey bars are guides to the eye.

3. Antiferromagnetic fluctuations as pairing glue for high-T_c superconductivity

We have reviewed above experimental information on the effect of compression on the superexchange interaction in cuprates. A brief summary of the most important findings is given below:

1. Compression of CuO_2 planes increases substantially superexchange interaction, according to Eq. (1) with $n \sim 10$, as long as there is no pressure-induced injection of charge carriers into CuO_2 planes. This is in stark contrast with earlier results (see above).

2. Doping of CuO_2 planes reduces superexchange interaction due to effective screening of Cu–O–Cu superexchange path in Cu–O–Cu–O square plaquettes.

3. As follows from the infrared absorption, the two-magnon, and higher (four magnon, six magnon, etc.), spin excitations at the Brillouin zone (BZ) boundary (antinodal part of the BZ), couple strongly to phonons. Such coupling may provide precursors to formation of stripes and similar lattice distortions (charge density waves?).

We will argue below, that with this information at hand we are ready to discuss pressure effects on the superconductivity and to make a selection of the most likely candidate, which provides a superconducting glue in cuprates and is behind the intriguing complexity of these materials.

It is evident from foregoing discussion that superexchange interaction is at the center of our discussion. It has been suggested as a relevant energy scale for the mechanism of high-T_c superconductivity from the early days since the discovery of T_c's of the order of 100 K, well above those provided by standard electron–phonon coupling mechanism. For the phonon-driven superconductor, Carbotte and Marsiglio [41] have estimated in a simplified Eliashberg approach the energy of the excitations which provide most effective (strongest) coupling required to optimize superconducting temperature. They have found that the optimum energy Ω_o is about 10 times higher than the superconducting transition temperature T_c. For modified McMillan formula [42] and optimum Ω_o (Einstein model) this would result in

$$T_c \cong \frac{1}{10}\Omega_o \sim \frac{\Omega_o}{1.2}\exp\left(-1.04(1+\lambda)/\lambda\right)$$

(Coulomb repulsion neglected). It immediately follows that $\lambda \sim 1$ is the coupling strength for such optimum coupling condition. In real materials, Einstein model (single oscillator with frequency Ω_o) does not hold, and the average phonon frequency entering McMilan's expression is an average over the phonon spectrum. For crude estimates, an expression $T_c = \Omega_{max}/20$, where Ω_{max} is a maximum phonon frequency, provides an order of magnitude estimate of superconducting temperature, for optimum electron–phonon coupling conditions. Similar expressions do not exist for the spin-fluctuation mechanism, but it is widely assumed that analogous expressions may be valid based on a similar Eliashberg-type equations for spin-driven superconductivity.

The energy scale given by two-magnon excitations in optimally doped Bi2212 cuprates [43] is $J \sim \omega(2M)/2.7 = 833$ K (573 cm^{-1}), which is almost two times less than in the parent compound ($J \sim 1150$ cm^{-1}). Application of the Eliashberg-type expression $T_c \cong \Omega_o/10$ for $\Omega_o = J$, gives $T_c = 83.3$ K, very close to the experimental value around 90 K. Existing calculations based on Hubbard model [44] provide an estimate $T_c \sim 0.3J = 250$ K, which is well above the experimental value. For estimates below, we will use empirical relation $T_c \sim 0.1J$, calculated for $T_c \sim 90$ K, $J = 833$ K. One of the missing parameters for discussion is doping dependence of J, which we derive from the paper by Sugai *et al*. [43] to be $dJ/d\delta = -6.4\cdot10^3$ K, δ — doping parameter, $\delta = 0.16$ for optimum doping [43]. It is interesting to note here that pairing temperature $T^* = 0.3J$, as estimated from the Hubbard model [44], follows closely pseudogap dependence [45] in Bi2212 material.

Now we have almost all the parameters at hand to discuss the pressure dependence of T_c in optimally doped material and relevance of superexchange interaction as a glue for superconductivity. We have used Eq. (1) to estimate the pressure dependence of J, and assumed that $dJ/d\delta = -6.4\cdot10^3$ K, and fitted $d\delta/dP = 2.5\cdot10^{-2}$ GPa^{-1} to match linear rise of T_c ($T_c \sim 0.104\,J$) in optimally doped material, which we measured earlier [46]. The result of the fit is shown in Fig. 5. Our model does not fit the experimental data in the whole pressure range, but the discrepancy is quite instructive. First, in the magnetic susceptibility data for this sample, signal starts deteriorating above 5 GPa (Fig. 5), and most of its intensity is lost at the highest pressure. Thus, the observed deviation may be due to real physical phenomena occurring in the sample, which is easy to overlook with simplistic phenomenological models explaining parabolic pressure dependence of T_c [46,47]. The observed sharp decrease of T_c may be due to strong deterioration of superexchange interaction. However, we believe that it is much more likely to be due to competing order, similar to a charge density wave state, which is competing with the superconducting state.

The competing order may be promoted by strong increase of coupling between magnetic and lattice degrees of freedom, similar to ones described above for phonon–magnon interactions revealed by infrared experiments. As a supporting argument, it is worth to mention recent experiments in single layer mercury cuprate [48], which demonstrated CDW-like state induced by high pressure, competing with the superconductivity. We would like to mention here that role of phonons is also supported by the evidence of soft-phonon scenario for CDW formation in the underdoped $YBa_2Cu_3O_{6.6}$ cuprate [49].

In summary, we have presented an overview of our experiments aimed at discovering details relevant to super-

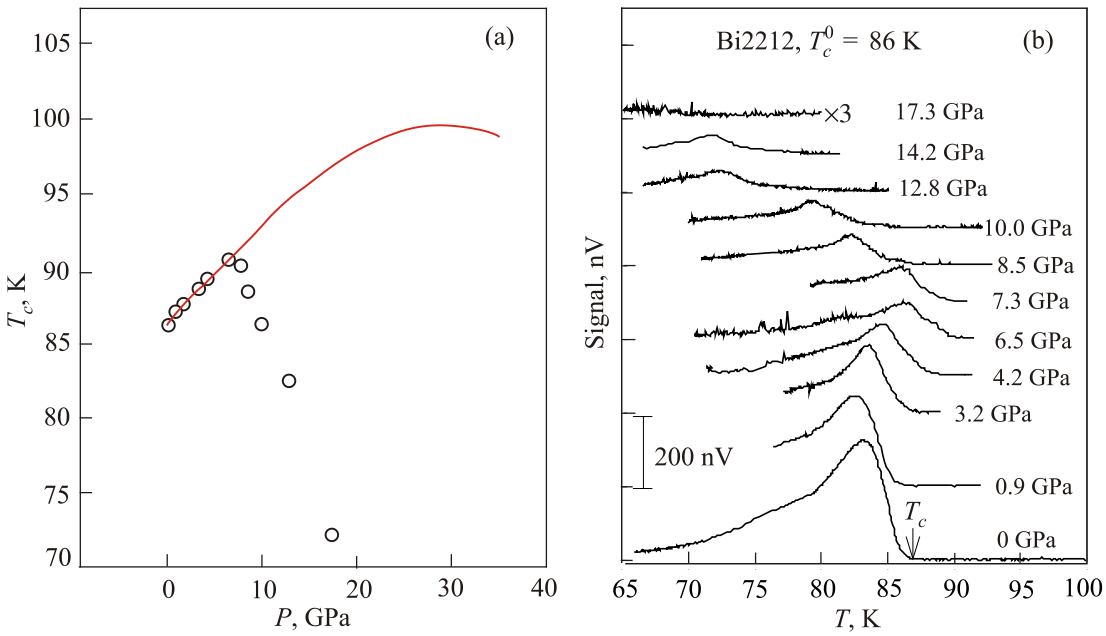

Fig. 5. T_c in optimally doped Bi2212 sample. (a) Experimental T_c values (open circles) and fit using values derived from superexchange based model. (b) Corresponding magnetic susceptibility signal. The magnitude of susceptibility response is significantly suppressed above 6.5 GPa.

exchange interaction as a driving force behind the mechanism of high T_c in cuprate materials. We have collected convincing evidence for the spin-driven mechanism of superconductivity, despite the fact that comprehensive theoretical explanation of the details of pairing in cuprates is still missing. The pressure variable is a natural tool which can be used to enhance superexchange interaction (Eq. (1)), providing an enhanced energy scale for electron pairing in compressed cuprates. Moreover, we believe that future work will help to clarify the role of phonon–magnon interactions in the CDW state observed in all the cuprate families of materials. At higher pressures, the increased coupling to the lattice should invariably favor formation of ordered CDW state (and, possibly, spin-density wave state) in cuprates due to increased coupling of magnetic excitations to the crystal lattice vibrations, which could lead to phonon softening effects [49].

Acknowledgments

This work was supported by DOE/BES under contract No. DE-FG02-99ER45775.

1. A.J. Achkar, R. Sutarto, X. Mao, F. He, A. Frano, S. Blanco-Canosa, M. Le Tacon, G. Ghiringhelli, L. Braicovich, M. Minola, M. Moretti Sala, C. Mazzoli, Ruixing Liang, D.A. Bonn, W. N. Hardy, B. Keimer, G. A. Sawatzky, and D.G. Hawthorn, *Phys. Rev. Lett.* **109**, 167001 (2012).
2. J. Chang, J. Chang, E. Blackburn, A.T. Holmes, N.B. Christensen, J. Larsen, J. Mesot, Ruixing Liang, D.A. Bonn, W.N. Hardy, A. Watenphul, M. von Zimmermann, E.M. Forgan, and S. M. Hayden, *Nature Phys.* **8**, 871 (2012).
3. G. Ghiringhelli, M. Le Tacon, M. Minola, S. Blanco-Canosa, C. Mazzoli, N.B. Brookes, G.M. De Luca, A. Frano, D.G. Hawthorn, F. He, T. Loew, M. Moretti Sala, D.C. Peets, M. Salluzzo, E. Schierle, R. Sutarto, G.A. Sawatzky, E. Weschke, B. Keimer, and L. Braicovich, *Science* **337**, 821 (2012).
4. E. Blackburn, E. Blackburn, J. Chang, M. Hücker, A.T. Holmes, N.B. Christensen, Ruixing Liang, D.A. Bonn, W.N. Hardy, U. Rütt, O. Gutowski, M. v. Zimmermann, E.M. Forgan, and S.M. Hayden, *Phys. Rev. Lett.* **110**, 137004 (2013).
5. D.H. Torchinsky, F. Mahmood, A.T. Bollinger, I. Božović, and N. Gedik, *Nat. Mater.* **12**, 387 (2013).
6. S. Blanco-Canosa, A. Frano, E. Schierle, J. Porras, T. Loew, M. Minola, M. Bluschke, E. Weschke, B. Keimer, and M. Le Tacon, *Phys. Rev. B* **90**, 054513 (2014).
7. R. Comin, A. Frano, M.M. Yee, Y. Yoshida, H. Eisaki, E. Schierle, E. Weschke, R. Sutarto, F. He, A. Soumyanarayanan, Yang He, M. Le Tacon, I.S. Elfimov, Jennifer E. Hoffman, G.A. Sawatzky, B. Keimer, A. Damascelli, *Science* **343**, 390 (2014).
8. M. Hücker, N.B. Christensen, A.T. Holmes, E. Blackburn, E.M. Forgan, Ruixing Liang, D.A. Bonn, W.N. Hardy, O. Gutowski, M. v. Zimmermann, S.M. Hayden, and J. Chang, *Phys. Rev. B* **90**, 054514 (2014).
9. E. Blackburn, *Phys. B: Condens. Matter* **460**, 132 (2015).
10. E. Fradkin, S.A. Kivelson, and J.M. Tranquada, *Rev. Mod. Phys.* **87**, 457 (2015).
11. B. Keimer, S.A. Kivelson, M.R. Norman, S. Uchida, and J. Zaanen, *Nature* **518**, 179 (2015).
12. G. Grüner, *Rev. Mod. Phys.* **60**, 1129 (1988).
13. P. Monceau, *Adv. Phys.* **61**, 325 (2012).

14. P.A.Fleury and R. Loudon, *Phys. Rev*. **166**, 514 (1968).
15. R.J. Elliott, and M.F. Thorpe, *J. Phys C: Solid State Phys*. **29**, 1630 (1969).
16. S. Sugai, S.-i. Shamoto, and M. Sato, *Phys. Rev. B* **38**, 6436 (1988).
17. K.B. Lyons, P.A. Fleury, J.P. Remeika, A.S. Cooper, and T.J. Negran, *Phys. Rev. B* **37**, 2353 (1988).
18. A.F. Goncharov and V.V. Struzhkin, *J. Raman Spectroscopy* **34**, 532 (2003).
19. M.J. Massey, N.H. Chen, J. W. Allen, and R. Merlin, *Phys. Rev. B* **42**, 8776 (1990).
20. V.V. Struzhkin, U. Schwarz, H. Wilhelm, and K. Syassen, *Mater. Sci. Engin. A* **168**, 103 (1993).
21. M.I. Eremets, et al. *JETP Lett*. **54**, 372 (1991).
22. V.V. Struzhkin, V.V. Struzhkin, A.F. Goncharov, H.K. Mao, R.J. Hemley, S.W. Moore, J.M. Graybeal, J. Sarrao, and Z. Fisk, *Phys. Rev. B* **62**, 3895 (2000).
23. R.R.P. Singh, P.A. Fleury, K.B. Lyons, and P.E. Sulewski, *Phys. Rev. Lett*. **62**, 2736 (1989).
24. M.C. Aronson, S.B. Dierker, B.S. Dennis, S.W. Cheong, and Z. Fisk, *Phys. Rev. B* **44**, 4657 (1991).
25. L.J. De Jongh and R. Block, *Physica B+C* **79**, 568 (1975).
26. S.L. Cooper, S.L. Cooper, G.A. Thomas, A.J. Millis, P.E. Sulewski, J. Orenstein, D.H. Rapkine, S.W. Cheong, and P.L.Trevor, *Phys. Rev. B* **42**, 10785 (1990).
27. V.J. Emery and G. Reiter, *Phys. Rev. B* **38**, 4547 (1988).
28. J.D. Perkins, J.M. Graybeal, M.A. Kastner, R.J. Birgeneau, J.P. Falck, and M. Greven, *Phys. Rev. Lett*. **71**, 1621 (1993).
29. M. Grüninger, M. Grüninger, J. Münzel, A. Gaymann, A. Zibold, H.P. Geserich, and T. Kopp, *Europhys. Lett*. **35**, 55 (1996).
30. J. Lorenzana and G.A. Sawatzky, *Phys. Rev. Lett*. **74**, 1867 (1995).
31. J. Lorenzana and G.A. Sawatzky, *Phys. Rev. B* **52**, 9576 (1995).
32. R. Newman and R.M. Chrenko, *Phys. Rev*. **114**, 1507 (1959).
33. H. Suzuura, H. Yasuhara, A. Furusaki, N. Nagaosa, and Tokura, *Phys. Rev. Lett*. **76**, 2579 (1996).
34. T. Cuk, T. Cuk, V.V. Struzhkin, T.P. Devereaux, A.F. Goncharov, C.A. Kendziora, H. Eisaki, H.K. Mao, Z.X. Shen, *Phys. Rev. Lett*. **100**, 217003 (2008).
35. B.S. Shastry and B.I. Shraiman, *Phys. Rev. Lett*. **65**, 1068 (1990).
36. J.K. Freericks and T.P. Devereaux, *Phys. Rev. B* **64**, 125110 (2001).
37. T.P. Devereaux, A. Virosztek, and A. Zawadowski, *Phys. Rev. B* **51**, 505 (1995).
38. M. Capone, M. Fabrizio, C. Castellani, and E. Tosatti, *Science* **296**, 2364 (2002).
39. S. Sugai and M. Sato, *Phys. Rev. B* **40**, 9292 (1989).
40. X.-J. Chen, X.-J. Chen, V.V. Struzhkin, Yong Yu, A.F. Goncharov, C.-T. Lin, Ho-kwang Mao, and R.J. Hemley, *Nature* **466**, 950 (2010).
41. J.P. Carbotte and F. Marsiglio, in The Physics of Superconductors, K.H. Bennemann and J.B. Ketterson (eds.), Ch. 4, 233, Springer–Berlin–Heidelberg (2003).
42. P.B. Allen and R.C. Dynes, *Phys. Rev. B* **12**, 905 (1975).
43. S. Sugai, H. Suzuki, Y. Takayanagi, T. Hosokawa, and N. Hayamizu, *Phys. Rev. B* **68**, 184504 (2003).
44. N.M. Plakida, L. Anton, S. Adam, and G. Adam, *JETP* **97**, 331 (2003).
45. M. Hashimoto, I.M. Vishik, R.-H. He, T.P. Devereaux, and Z.-X. Shen, *Nature Phys*. **10**, 483 (2014).
46. X.-J. Chen, V.V. Struzhkin, R.J. Hemley, H.-k. Mao, and C. Kendziora, *Phys. Rev. B* **70**, 214502 (2004).
47. J.L. Tallon, C. Bernhard, H. Shaked, R.L. Hitterman, and J.D. Jorgensen, *Phys. Rev. B* **51**, 12911 (1995).
48. M. Izquierdo, D.C. Freitas, D. Colson, G. Garbarino, A. Forget, S. Megtert, H. Raffy, R. Comes, J.-P. Itié, S. Ravy, P. Fertey, and M. Núñez-Regueiro, *arXiv:1510.03750* [*cond-mat.supr-con*] (2015).
49. M. Le Tacon, M.Le Tacon, A. Bosak, S.M. Souliou, G. Dellea, T. Loew, R. Heid, K.-P. Bohnen, G. Ghiringhelli, M. Krisch, and B. Keimer, *Nature Phys.* **10**, 52 (2014).